Curli-Mediated Self-Assembly of a Fibrous Protein Scaffold for Hydroxyapatite Mineralization

Zahra Abdali, Masoud Aminzare, Xiaodan Zhu, Elizabeth DeBenedictis, Oliver Xie, Sinan Keten, Noémie-Manuelle Dorval Courchesne*

Abstract

Nanostructures formed by self-assembled peptides have been increasingly exploited as functional materials for a wide variety of applications, from biotechnology to energy. However, it is sometimes challenging to assemble free short peptides into functional supramolecular structures, since not all peptides have the ability to self-assemble. Here, we report a self-assembly mechanism for short functional peptides that we derived from a class of fiber-forming amyloid proteins called curli. CsgA, the major subunit of curli fibers, is a self-assembling β-helical subunit composed of five pseudo-repeats (R1-R5). We first deleted the internal repeats (R2, R3, R4), known to be less essential for the aggregation of CsgA monomers into fibers, forming a truncated CsgA variant (R1/R5). As a proof-of-concept to introduce functionality in the fibers, we then genetically substituted the internal repeats by a hydroxyapatite (HAP)-binding peptide, resulting in a R1/HAP/R5 construct. Our method thus utilizes the R1/R5-driven self-assembly mechanism to assemble the HAP-binding peptide and form hydrogel-like materials in macroscopic quantities suitable for biomineralization. We confirmed the expression and fibrillar morphology of the truncated and HAP-containing curli-like amyloid fibers. X-ray diffraction and TEM showed the functionality of the HAP-binding peptide for mineralization and formation of nanocrystalline HAP.

Overall, we show that fusion to the R1 and R5 repeats of CsgA enables the self-assembly of functional peptides into micron long fibers. Further, the mineral-templating ability that the R1/HAP/R5 fibers possesses opens up broader applications for curli proteins in the tissue engineering and biomaterials fields.

Keywords: self-assembling proteins, curli fibers, hydroxyapatite-binding peptide, supramolecular protein materials, biomaterials, biomineralization.

Curli fibers are a group of functional amyloids assembled by many Gram-negative bacteria, such as *E. coli*, as part of their extracellular matrix.[1, 2] Curli fibers are composed of repeated self-assembling subunits, called CsgA, which consist of a β-helix structure composed of five pseudo-repeats (R1-R5). Each repeat comprises two β-strands on opposite sides of the protein, which adopts an overall β-helical tertiary structure.[1, 2] Due to this characteristic β-helical structure and their high propensity to aggregate after extracellular secretion, self-assembled CsgA proteins form mechanically and chemically resistant amyloid fibers. Furthermore, these fibers are extremely versatile for customization with functional domains – the protein core of CsgA can be directly mutated,[3, 4] and the protein can be genetically fused with small peptides or large protein domains for a wide variety of applications.[5-8]

Although the five repeats of CsgA have very similar sequences, it has been found that only the external N- and C-terminal repeats are crucial for CsgA self-assembly and seeding.[2, 9] Wang *et al*, studied the polymerization rate of different repeat-deletion CsgA mutants using Thioflavin T fluorescence.[9] They observed a defective polymerization for R5-deleted CsgA with a long lag phase (~ 25 h) compared with other mutations. In contrast, the polymerization of CsgA mutants

with removed R2, R3, or R4 was not impaired, but showed a longer lag phase (~ 2 h) compared with WT CsgA (~ 1 h). Besides, studying the polymerization of chemically synthesized monomers showed no detectable lag phase for R5, a shorter lag phase for R1 compared with R3 (2 times shorter), and no polymerization for R2 and R4 after removal of the denaturant. These observations indicate the greatest contribution of R1 and R5 to protein aggregation compared with the internal repeats. Collectively, these results demonstrated that R1 and R5, the N- and C-terminal external repeats of CsgA, play an important role in the self-polymerization of CsgA, while R2, R3, and R4 are not essential for amyloid formation.

These observations raise the questions of whether a synthetic truncated CsgA-like protein (with deleted internal repeats) could retain the ability to assemble into amyloid fibers, and whether this new CsgA-like self-assembling scaffold (consisting of R1 and R5) could be used as a minimum required structure to drive the assembly of protein materials. The unique ability of a truncated CsgA to self-assemble into fibers, and to aggregate into supramolecular materials and hydrogels [5, 10, 11] could be employed to mediate the assembly of functional peptides or proteins that do not have the ability to self-assemble by themselves. Motivated by this hypothesis, here we report the deletion of the R2, R3, and R4 pseudo-repeats of CsgA and the study of the assembly of the new truncated CsgA (R1/R5). We further replaced the internal repeats by a functional peptide to utilize the R1/R5-driven self-assembly mechanism to assemble non-amyloidogenic functional protein domains (Figure 1A). We chose to replace the internal repeats of CsgA with a functional peptide - rather than fusing the peptide to the N- or C-terminus of the truncated CsgA - in order to minimize steric hindrance of the fused domain. In fact, it has been reported that the fusion of protein domains at N- or C-terminus of CsgA can affect assembly rate, morphology, and stiffness

of the resultant fibrils by interfering with monomer interactions.[12] Substituting the internal repeats with a peptide also allows for introducing new functionalities in curli-like fibers. In addition, truncating CsgA could provide the opportunity of fusing large proteins that may otherwise be challenging to secret extracellularly through the native CsgA secretion pathway. As a proof of concept, we used a short 12-amino acid peptide that has a specific binding affinity to single-crystal hydroxyapatite (HAP), and that can template the nucleation and growth of crystalline HAP.[13] HAP is the main component of bone, acting as a template for the mineral phase deposition and stimulating new bone formation.[14] The HAP-binding peptide sequence resembles the tripeptide repeat (Gly-Pro-Hyp) of type I collagen, a major component of bone extracellular matrix. The main factor promoting specific interactions between the binding peptide and single-crystal HAP is the unique spatial arrangement of the residues in the HAP-binding site. Cooperative interactions of hydrogen bonding, van der Waals, and Coulombic types between the peptide and the HAP surface are other key contributing factors to increase the HAP binding.[13] Recently, hydrogels loaded with HAP were reported to show high osteointegration because of the spontaneous formation of a gel/bone hybrid layer at the interface of bone and scaffold that could effectively induce the osteogenic differentiation of human mesenchymal stem cells.[14-16] Among the methods of preparing mineralized scaffolds, soaking the scaffold in simulated body fluid (SBF) is the most commonly used surface mineralization technique.[17] However, it is difficult for the solution to reach the interior of the nanofibrous block, thus resulting in surface mineralization with randomly oriented clusters of the HAP crystals, as opposed to a bulk mineralization.[18]

Self-assembled peptide nanostructures have been increasingly exploited as functional materials for applications in biomedicine and energy.[19-22] To assist with the assembly of the free peptides,

physical or chemical tethering within the non-natural organic compounds, such as hydrophobic long chain alkyl or aromatic molecules, has been employed.[19] For instance, HAP-binding peptides have been chemically conjugated with hydrophobic alkyl chains to fabricate nanofiber-forming amphiphilic peptides that can assemble into hierarchically organized functional biomaterials.[23] Due to complexities associated with chemical conjugation, such as harsh and destructive reagents, weak bonding, change in peptides positioning after assembly, and low control over unwanted side reactions, genetic modifications open up new possibilities to engineer self-assembly of functional free peptides. Hence, our use of the curli self-assembly system to form fibers containing the HAP-binding peptide provides a means for genetically programming the self-assembly process without the need for chemical post-modifications. The self-assembled nanofibrous materials proposed here are suggestive to develop biomimetic materials, because they are similar to extracellular matrices as they display the high densities of biochemical cues and provide physical cues due to the unique geometry of the nanofibrous structures.[23] Fusing the HAP-binding peptide with each R1/R5 monomers, will further increase the density of the HAP nucleation sites and could facilitate bulk mineralization of the biomaterials.

Our work here verifies the hypothesis that a truncated CsgA can still self-assemble into curli-like fibers, and that the assembly of the HAP-binding peptide can be driven by the R1 and R5 repeats of CsgA. We characterized the secondary structure of these genetically engineered proteins and the aggregation and assembly behavior of the fibers. We also confirmed the functionality of the HAP-binding site incorporated into the protein fibers by comparing the HAP mineralization of the unmodified, truncated, and HAP-containing curli fibers as templates. This work opens up a new

direction to use the self-assembling behavior of the curli system to mediate the formation of protein fibers with other functional peptides.

Results and discussion

Expression and morphological characterization of curli-like protein fibers

To confirm the expression of engineered proteins and their assembly into curli-like fibers, we first used the Congo Red amyloid-binding dye and studied the expression of amyloid fibers quantitatively and qualitatively (Figure 1B). Cells expressing the modified CsgA proteins showed binding to Congo Red comparable with cells expressing WT curli fibers (positive control), and significantly higher compared with cells expressing maltose-binding proteins (MBP) (negative control). R1/HAP/R5 and R1/R5 showed 17% more and 15% less binding to Congo Red compared with the WT curli fibers. The greater dye binding capacity of R1/HAP/R5 could be due to non-specific binding of Congo Red to HAP-binding peptide or linker, and the lower dye binding by R1/R5 could be a result of the weaker tendency of R1/R5 proteins to aggregate to form bundles (refer to the upcoming discussion on structure self-assembly of R1/R5), thus entrapping fewer dye molecules. Although the expression of the R1/R5 was lower than WT, the yield of the isolated protein was still sufficient to support the fabrication process of protein hydrogels, thin films and mineralized hydrogels (Figure S2). Second, we also showed the deposition of assembled curli-like fibers on filter membranes during the filtration process. All filter membranes that served for filtering WT, truncated or HAP-containing curli-like fibers showed a red color after incubation with Congo Red, indicating the presence of amyloid fibers retained on the membranes. These results

indicate that the modified CsgA proteins can assemble into curli-like amyloid fibers, despite the deletion of internal R2, R3, and R4 repeats.

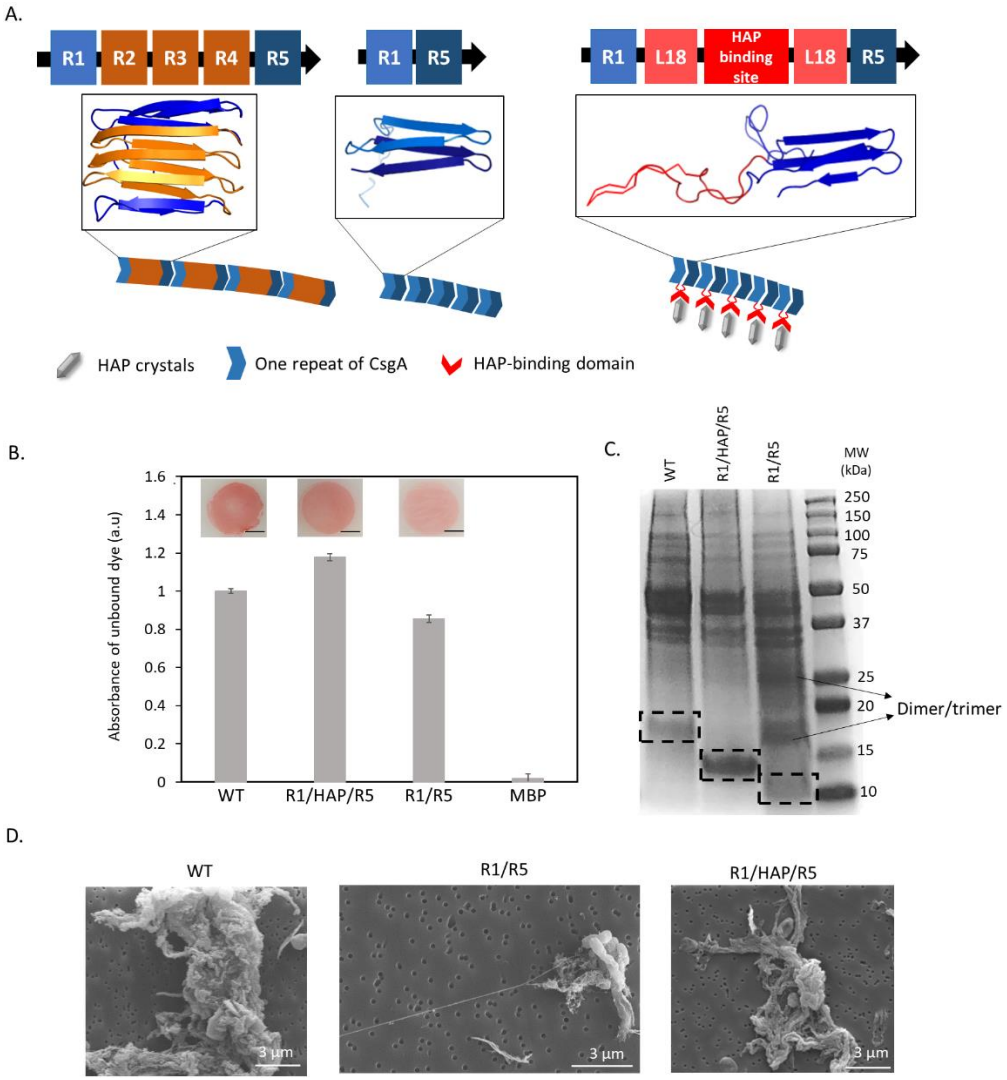

Figure 1. Expression of modified curli-like protein fibers assembled via R1-R5 interactions. (A) Proposed constructs for curli-like proteins (top) and their expected structures and assembly into fibers (bottom). (B) Qualitative and quantitative assessment of curli-like proteins expression using Congo Red staining method by staining the deposited proteins on filter membranes after vacuum filtration (top pictures), and by measuring the absorbance of unbound dye to protein expressing culture (absorbance values). Absorbance values were normalized by the cell density (A 490/ A 600) and relative to WT. Scale bars = 2 mm. (C) SDS-PAGE analysis of the semi-purified proteins showing bands of the expected molecular weight for wild type and modified CsgA proteins (black dash boxes), and bands for the dimer and trimer of R1/R5 (black arrows), (D) SEM images of bacterial cultures expressing curli-like proteins, showing bacterial cells and fibrous protein aggregates. Scale bars = 3 µm.

To further characterize the modified CsgA proteins, we isolated the proteins using vacuum filtration and obtained hydrogel proteins for all mutants (Figure S2). The yield of semi-purified curli fibers obtained via vacuum filtration has been determined previously to be around 50 mg per liter of culture, for filtration on 47 mm diameter filter membranes, with a purity as high as 80%. [6] We collected the products and confirmed the expression of each modified protein using SDS-PAGE to assess the presence of proteins with the predicted molecular weight (Figure 1C). We observed bands at molecular weights close to those expected for all three CsgA-like proteins (WT: 14.7 kDa, R1/HAP/R5: 10.9 kDa, R1/R5: 7.8 kDa), confirming the expression of the proteins, the deletion of the internal repeats for R1/R5, and their substitution with the HAP construct for R1/HAP/R5. In the case of R1/R5, additional bands were visible around 17 kDa, and around 25 kDa. These bands appeared to correspond to dimers and trimers of R1/R5 (close to the expected MW of dimers, ~16 kDa, and trimers, ~24 kDa), respectively. The fact that these bands are clearly observed in this lane only could indicate that short oligomers of R1/R5 proteins are more resistant to disassembly by incubation in a mixture of HFIP and TFA compared with larger curli subunits (CsgA or R1/HAP/R5), or that they can re-assemble faster when resuspended in an aqueous buffer. Additional bands of higher molecular weights observed in all three lanes correspond to others *E. coli* proteins (impurities) or CsgA oligomers.

We then analyzed the morphology and aggregation behavior of curli-like fibers after extracellular secretion using SEM (Figure 1D). SEM images of bacterial cultures (Figure 1D) show that all proteins exhibit fibrous structures that tend to aggregate together to form micron-sized bundles. The modified CsgA monomers thus retained the ability to self-assemble into fibrils, in a very similar fashion compared with WT CsgA. However, R1/R5-based fibers formed slightly less

aggregated and longer fibers. This weaker tendency of R1/R5 monomers to aggregate laterally and form large structures was consistent with our observation that milder conditions and shorter incubation times were necessary during vacuum filtration to retain the proteins on the filter membrane and obtain a high fiber isolation yield. Overall, the SEM images support the results obtained from the Congo Red binding assay and the fact that the modified proteins can assemble into fibrous structures after secretion into the extracellular medium. Although we deleted three internal repeats from the CsgA monomer, R1 and R5 still drive the assembly and interactions between the truncated monomers, thus serving as a template for assembly of the HAP-binding peptide. This short peptide does not spontaneously self-assemble into higher order structures, but R1 and R5 enabled its assembly into supramolecular fiber-like structures. Besides, the modified proteins exhibited a fibrillar extracellular matrix-like structure with a porous hydrogel microarchitecture that has proven to be important for potential applications, such as bone tissue engineering, that involves in cell integration.[24]

Next, we decided to further probe the differences in fiber length and aggregation of the modified proteins by analyzing the morphology and re-assembly kinetics of disassembled fibers using atomic force microscopy (AFM) (Figure 2). To study the effect of time on the fibrillation of the monomers, we allowed disassembled monomer solutions to re-assemble in DI water for 20 s, 20 min, and 3 h (enough time for WT CsgA monomers to fibrillate into an extended network of fibrils), and cast the mixture onto mica for AFM imaging. Immediately after mixing with water, CsgA and CsgA-like monomers began forming short filaments. After 3 h, WT monomers still appeared as relatively short fibrils, with a maximum length of around 200 nm. The R1/HAP/R5 monomers polymerized into slightly longer fibers, ranging between 200 and 500 nm in length. In

contrast, R1/R5 monomers showed a faster growth and fibrillation even after a short incubation time. After 20 min, we observed fibers of over 2 µm in length. The formation of truncated CsgA fibrils therefore supports the hypothesis that removing the internal repeats of CsgA does not compromise self-assembly, and that instead it promotes the formation of longer fibers. Indeed, as previously reported,[2, 9] R1 and R5 are the most aggregation prone repeats of CsgA and can drive the assembly of amyloid fibers. These observations combined with the rapid di/trimerization of the R1/R5 monomers observed by SDS-PAGE further illustrated the fast re-assembly of truncated CsgA proteins into fibers.

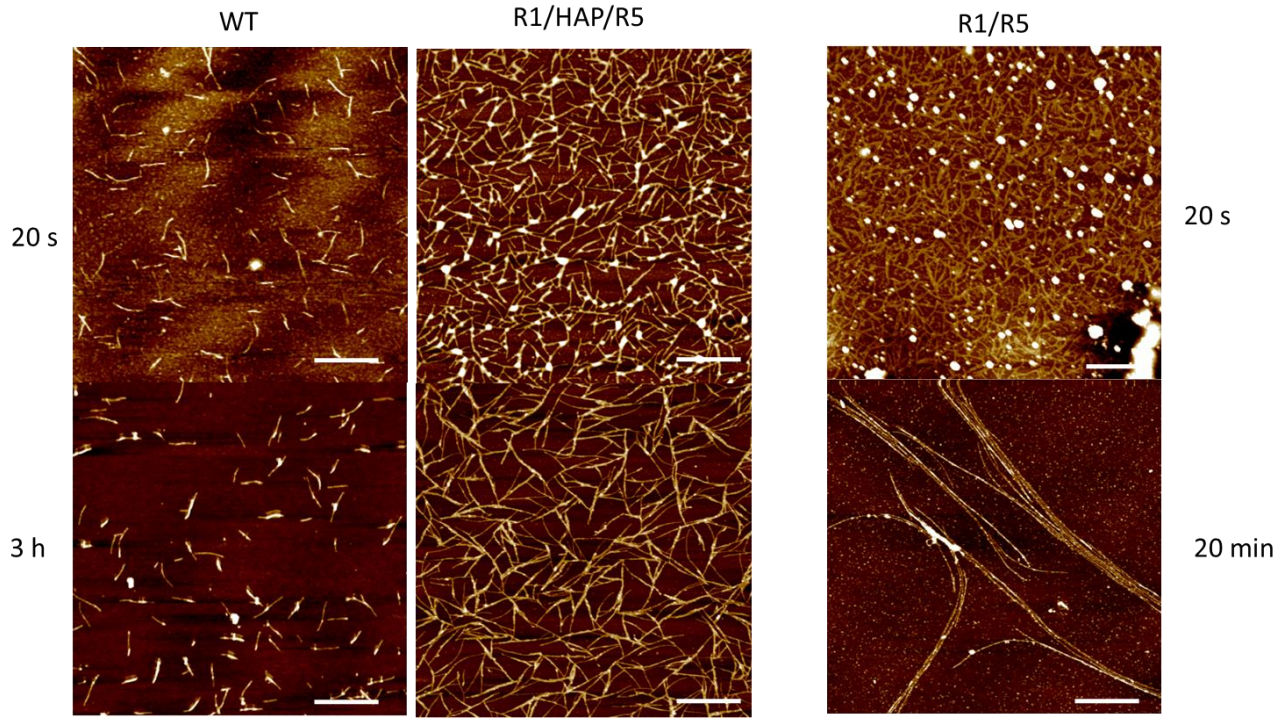

Figure 2. AFM micrographs of curli-like fibers after re-assembling with different growth times in water. Significantly long fibers formed after re-assembly of the R1/R5 within 20 min. Scale bar is 500 nm.

Structural characterization and modelling of modified CsgA proteins

To investigate the folding of individual curli-like proteins and their oligomers, we studied their secondary, tertiary and quaternary structures using experimental and modelling techniques. First, to find out whether the mutated proteins folded into the characteristic secondary structure of the CsgA after modification, we studied their structure using circular dichroism (CD) (Figure 3A). We observed a characteristic minimum in the range of 215-220 nm and maximum in the range of 188-191 nm exhibiting strong β-sheet signatures for all the modified proteins. The β-helical fold of CsgA proteins is supported by the extensive hydrogen bond network between the amino acids on the adjacent strands .[25, 26] The intensity of the characteristic peak around 215 nm is slightly lower for R1/HAP/R5 than for WT and R1/R5, which is likely due to the incorporation of the HAP-binding peptide in the truncated CsgA monomer. The random coil structure of the HAP-binding peptide and flexible linkers could lower the intensity of the β-sheet signature peaks.[13] Besides, the HAP-binding peptide and the flexible linkers could also disrupt some of the inter-strand hydrogen bonds between R1 and R5, and therefore the overall stability of the protein. Nevertheless, the interactions between the side chains, such as polar interactions and hydrogen bonding, are still abundant to support the formation of the β-sheet.

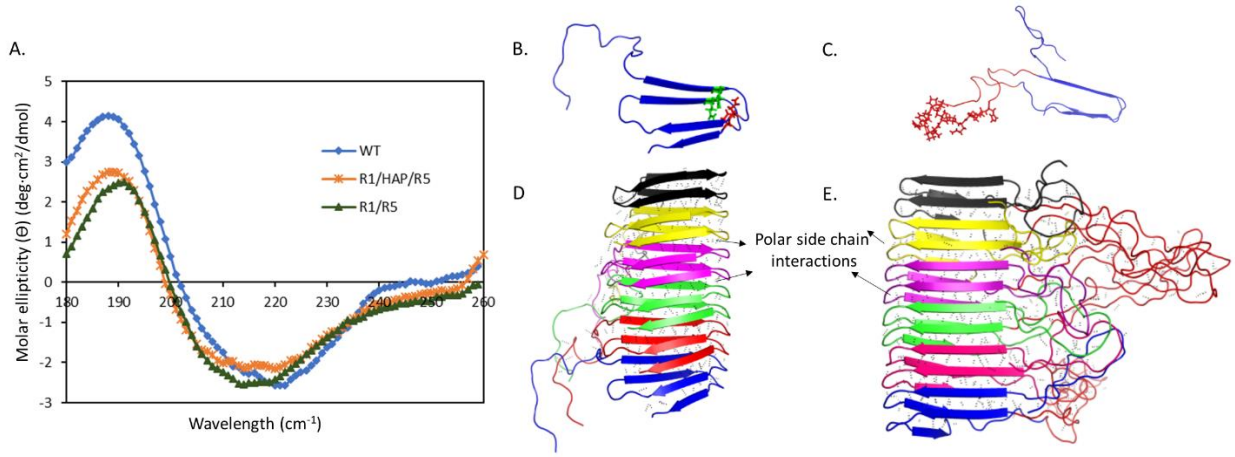

Figure 3. Structural characterization and modelling of curli-like proteins. (A) CD spectrum of the modified proteins showing characteristic peaks indicating strong β-sheet signatures for all proteins. (B through E) Molecular dynamic models of the (B) R1/R5 monomer, mapped onto R1/R2 of the wild type CsgA monomer, showing aligned Gln7 (green) and Asn12 (red), (C) R1/HAP/R5 monomer (top view) with fused flexible linker and HAP-binding peptide, (D) R1/R5 6-mer and (E) R1/HAP/R5 6-mer minimized and equilibrated in implicit solvent in NAMD.

To investigate the tertiary and quaternary structures of truncated CsgA subunits, we developed a monomer model with the R2-R4 repeats removed and stacked the truncated monomers to build oligomers (Figure 3B, D). We also constructed a variant with the HAP protein inserted between repeats R1 and R5 (Figure 3C, E). The R1 and R5 β-strand repeats are aligned as in Chapman's proposed β-helical model of CsgA,[1] only with the middle R2-R4 repeats missing. In these multimers, β-sheets still form across adjacent monomers and conserved polar residues inside the amyloid core (Ser, Gln, Asn) remain aligned, including preservation of the four residues critical for self-assembly in WT CsgA (Q29, N34, Q119, and N124).[27]

The β-sheet secondary structure is also maintained with the addition of the HAP protein between the R1 and R5 repeats. The HAP protein is modeled as unstructured and positioned to the side of the amyloid core, connected by flexible linkers. While β-sheets across the R1/R5 strands still form, it is possible that the incorporated HAP proteins may interact with the amyloid core, disrupting β-strand hydrogen bonding and the stability of the core. It is also possible that the bulky insertion may eventually split apart the β-sheet faces nearest the HAP protein slightly. While the β-helical structure is preserved in these variants, the self-assembly process likely differs. The R1 and R5 repeats direct the polymerization of WT CsgA,[28] while R2-R4 contain multiple "gatekeeper" residues (of aspartic acid or glycine) that slow curli growth of WT CsgA.[29] The removal of the R2-R4 beta strands includes removing charged residues from the β-sheet surface and turn regions.

WT CsgA typically has a -6e charge, removing strands R2-R4 means removing 8 negatively charged residues and 3 positively charged residues variants, resulting in a net change of +5e from the WT CsgA and a total charge of -1e in the R1/R5 variants. While molecular-level details of fiber aggregation are not currently known, we expect that changing the charge distribution on the surface of the monomers will impact (and potentially impede) self-assembly and bundled structure. We also anticipate that including the HAP protein will alter bundle formation as fibril diameter has been shown to increase with the molecular weight of proteins fused to CsgA.[30] Previous investigation of CsgA-fusion proteins found the fibers still able to self-assemble, although with slower growth.[30] Overall, both the experimental circular dichroism data and our modelling predictions indicate that truncated CsgA subunits adopts a β-helical fold that resembles that of WT CsgA.

Mineralization of curli-like proteins with HAP crystals

To analyze the functionality of the HAP-binding peptide integrated in the R1/HAP/R5 fibers, we performed mineralization studies on all three protein types. We compared the mineralized R1/HAP/R5 fibers with mineralized WT CsgA and truncated CsgA fibers in terms of composition, mineral density, and crystallinity.

To mineralize R1/HAP/R5 fibers, we first attempted to submerging the protein hydrogel in simulated body fluid (SBF). However, mineralization in SBF resulted in inhomogeneous and surface-only distribution of crystalline particles. The formation of large particles (2-3 microns) of various shapes (rod, flakes, hexagonal) indicated a rapid and uncontrolled deposition of minerals on the surface of the sample, with limited diffusion of calcium and phosphate ions into the bulk

of the hydrogel (Figure S3.A). Second, to dilute the fibers and allow for *in situ* mineralization during expression, we attempted to mineralize the fibers directly in the culture medium as bacteria express the proteins by adding SBF to the culture. However, this method resulted in a two-fold lower protein expression (verified by a Congo Red pull-down assay) compared with proteins expressed in the absence of SBF, and in a low density of the mineral deposition on the proteins (Figure S3.B). Third, we mineralized the proteins using $CaCl_2$ and Na_2HPO_4 precursors instead of SBF, which yielded a uniform and dense formation of nano-sized minerals (Figure 4A and S3.C). Using this optimized method, we obtained a uniform deposition of the HAP nanostructures alongside the fibers. SEM images also show that the porous fibrous structure of the protein hydrogels was preserved after mineralization, a feature that would be important for using the mineralized scaffolds for bone tissue engineering applications. Furthermore, we confirmed the formation of HAP crystals in the interior of the hydrogels by analyzing the cross-sectional morphology of the mineralized R1/HAP/R5 (Figure S4).

To verify the crystallinity of these HAP nanostructures, we obtained the XRD pattern of the R1/HAP/R5 composite (Figure 4B). The penetration depth of energetic X-rays within a sample is on the scale of ≈ 100 μm,[31] thus providing information about crystallinity within the bulk of the sample rather than the surface only. The XRD pattern of the mineralized proteins showed sharp peaks at 27.4°, 31.8°, 36.6°, and 45.7°, characteristic of crystalline HAP, which are assigned to (211), (300), (113), and (002) planes and are an indication of the crystallization of the hydrogel with HAP.[14, 32]

To better compare the extent of mineral formation onto the R1/HAP/R5 fibers with WT and R1/R5 fibers, residual salts and non-specifically bound HAP needed to be thoroughly washed off the

samples prior to imaging. Therefore, we adapted a different protocol with a lower concentration of proteins and mineralization solution for TEM analysis. Figure 4C shows images of curli-like proteins mineralized directly on TEM grids, along with a control grid incubated in the mineralization solution only (no proteins). We first used a control without proteins to determine how HAP would nucleate on the TEM grid without a protein template. We observed no formation of the crystalline HAP on these protein-free grids, highlighting the importance of protein templating for nucleation and crystal growth. Next, R1/R5-coated grids showed aggregates of particles, which we later characterized as amorphous particles. In contrast, TEM grids coated with R1/HAP/R5 and WT curli fibers showed substantial growth of flake-like crystals. We obtained dense aggregations of the flake-like particles of approximately 200 nm in the presence of R1/HAP/R5 nanofibers. While the density of HAP crystals was higher for R1/HAP/R5 fibers compared with WT, WT hydrogel also served as template for the growth of HAP. The formation of HAP flakes (layers) onto WT proteins could be due to the presence of the charged amino acids in WT CsgA. Removing the internal repeats of CsgA resulted in removing the majority of the anionic amino acids (aspartic acid, glutamic acid) and cationic amino acids (arginine, histidine, and lysine). Charged amino acids are attracted to Ca^{2+} and PO_4^{3-} ions and promote HAP precipitation and the local supersaturation.[33] Therefore, they provide energetically favorable binding sites for the initial nucleation (and growth) of the minerals, which results in more stable and crystalline HAP nanoparticles. As a result, the R1/R5 protein, which lacks the favorable binding sites, showed no crystalline phase. Although we removed the internal repeats in the R1/HAP/R5 proteins, they are effective templates for formation of crystals. The dense and homogeneous deposition of the HAP nanocrystals in the mineralized R1/HAP/R5 was due to the incorporated HAP-binding peptides.

Specific affinity of the HAP crystals to the binding peptide, along with the hydrogen bindings and electrostatic interactions, induced more specific and stable interaction as well as higher concentrations of the HAP nanocrystals with R1/HAP/R5.

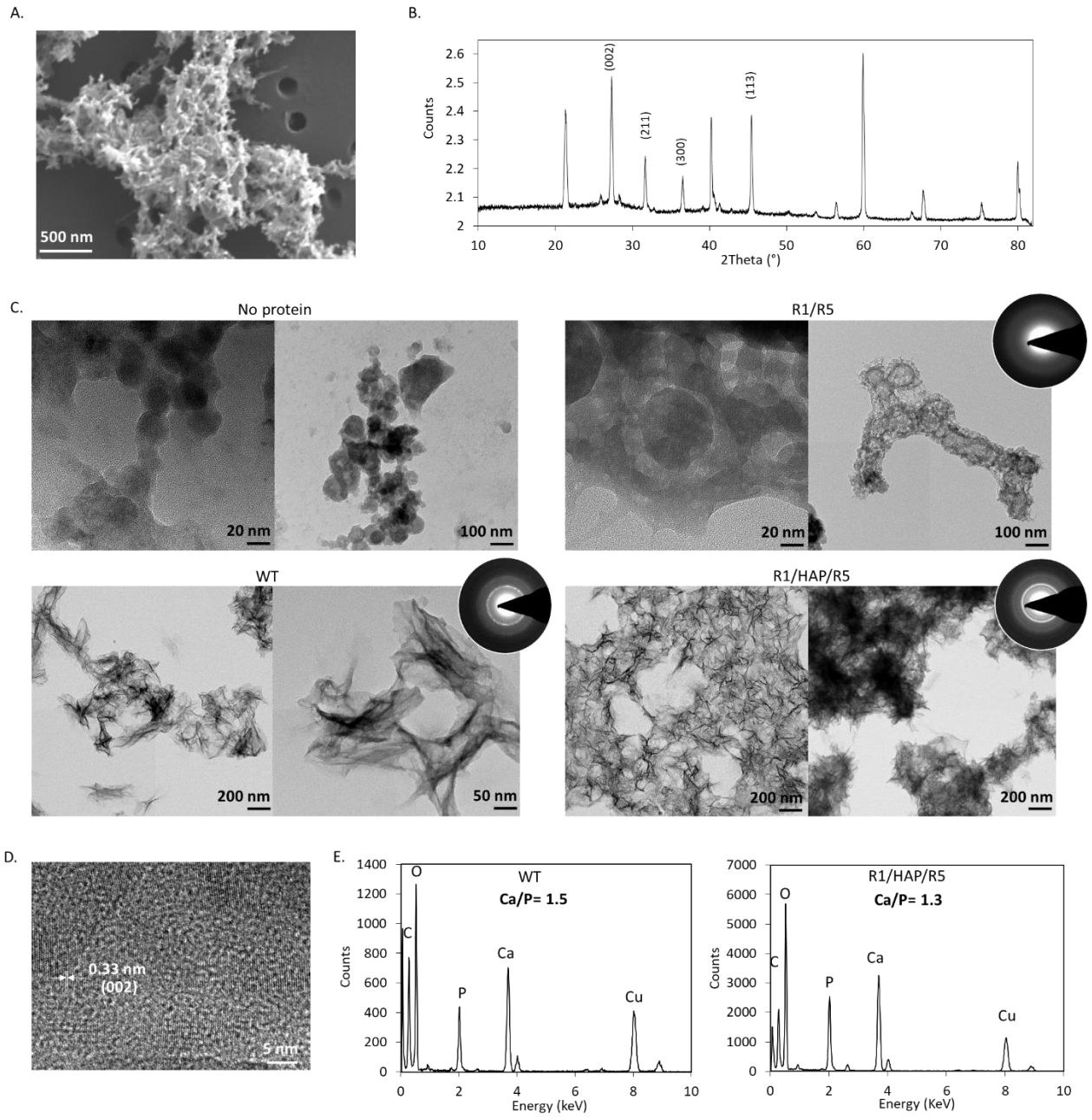

Figure 4. Characterization of curli-based proteins mineralized with hydroxyapatite. (A) SEM image and (B) XRD spectrum of mineralized R1/HAP/R5 protein fibers. (C) HAP mineralized directly on TEM grids, without template (top left), and with protein fibers as templates (R1/R5, WT and R1/HAP/R5). TEM images show

HAP nanoflakes formed by WT and R1/HAP/R5 proteins. SEAD patterns are shown for protein-templated HAP. Continuous rings are indicative of crystalline phase. (D) TEM image showing the interplanar spacing corresponding to the (002) plane of HAP nanoflakes. (E) EDS spectra highlighting the Ca/P ratio in the protein-templated HAP samples.

To compare the crystallinity of the minerals onto different protein templates, we obtained the selected area electron diffraction (SAED) patterns of the mineralized samples (Figure 4C). R1/R5 with a halo pattern and R1/HAP/R5 with a sharp continuous arc-shaped pattern demonstrated the amorphous and crystalline phases of these samples, respectively.[18] The R1/R5 protein template generated amorphous HAP without any clear SAED pattern, while characteristic patterns confirmed the crystalline HAP mineral phase in the R1/HAP/R5-templated sample. When comparing R1/HAP/R5 with WT, we observed distinct diffraction rings for the R1/HAP/R5 sample corresponding to the hexagonal phase of HAP. The intensity of the diffraction rings in R1/HAP/R5 is indicative of the highly crystalline nature of the sample. In contrast, the SAED pattern for WT-templated HAP showed discrete spotted rings, indicating that WT proteins produce HAP crystals with a broader size distribution compared with R1/HAP/R5.[34] In addition, the interplanar spacing of 0.33 nm between the HAP lattice places in the R1/HAP/R5-HAP nanocomposites (observed by TEM, Figure 4D) were ascribed to the (002) plane of HAP nanoflakes, further confirming the expected HAP crystal structure.[35] Together, these results indicate that the HAP-binding peptide plays an important role for directing the nucleation and growth of crystalline HAP in the modified curli-like fibers.

Finally, we investigated the composition of the protein-HAP samples by performing EDS analyses of the TEM samples. These analyses confirmed the presence of HAP templated by WT and R1/HAP/R5 proteins through a quantification of the calcium and phosphorus present in the

mineralized proteins (Figure 4E). The theoretical Ca/P atomic ratio for HAP ($Ca_{10}(PO_4)_6(OH)_2$) is 1.67, which corresponds roughly to the ratio calculated via EDS in the mineralized R1/HAP/R5 and WT (1.3 and 1.5, respectively).[36] It should be noted that EDS approximately characterizes only the surface of the sample and that the Ca/P ratio could change with airborne contaminations or any remaining ions (PO_4^{3-} and Ca^{2+}) adsorbed on the surface, explaining the slight differences with the theoretical ratio. Overall, the similarity between the experimental and predicted ratios suggests that the nanoflakes are truly HAP nanocrystals.

Collectively, the mineralization results confirm the functionality of the HAP-binding peptide incorporated in the truncated CsgA subunit. We observed a greater density of HAP crystals for the R1/HAP/R5 samples compared with WT CsgA and truncated R1/R5 proteins. Therefore, the incorporation of the HAP-binding peptide is an opportunity to use the curli-like fibers as a template for mineralization for various applications.

Materials and methods

Cell strains, plasmids, and curli expression. The pET21d-*csgACEFG* plasmid and the curli operon deletion mutant strain of *E. coli*, PQN4,[6] were gifts from the Joshi Lab (Harvard University, Boston, MA). We used this pET21d plasmid, with the curli operon (without the CsgB nucleator protein) under the control of the T7 promoter, as template vector to synthesize different genetic variants of the CsgA protein. To truncate wild-type CsgA (WT), whole CsgA fragment was replaced with a modified CsgA (R1/R5) fragment consisting only R1 and R5 (Life technologies) using Gibson assembly (New England Biolabs). The pET21d-*csgACEFG* plasmid was linearized using forward and reverse primers starting at the C-terminal end of the CsgA and at the end of N22, respectively.

The double-stranded DNA fragment of encoding R1/R5 was inserted in the linearized plasmid. To remove the internal repeats and replace with the HAP-binding peptide, the pET21d-*csgACEFG* plasmid was linearized using forward and reverse primers starting at the beginning of R5 and at the end of R1, respectively. The oligonucleotide (108 bp) encoding HAP-binding peptide, with two flexible glycine-serine linkers (L12) at the C- and N-terminals of HAP, was synthesized by overlap elongation PCR and inserted in between R1 and R5 using Gibson assembly (R1/HAP/R5). Based on the size of the fusion domain used here (HAP binding site: 12 residues), we selected (GSG)4 (L12) as a linker with a reasonable length and flexibility to guarantee the availability of the binding peptide. A six-histidine tag (HisTag) was added to the C-terminus of all the WT and modified CsgA monomers to allow for immunodetection. A pET21d plasmid containing the *malE* gene was used to express maltose-binding proteins (MBP) as a negative control for amyloid formation. Sequences of the all the genes and primers are listed in supporting information (Table S1 and Figure S1).

To express the proteins, the transformed PQN4 cells were streaked onto lysogeny broth (LB) agar plates containing 100 μg/mL carbenicillin and 0.5% (m/v) glucose (for catabolite repression of T7RNAP). Colonies were picked from the plates, and 5 mL cultures were inoculated (in LB containing and 100 μg/mL carbenicillin and 2% (m/v) glucose). Cultures were grown overnight at 37 °C. The overnight cultures were diluted 100-fold in fresh LB medium with 100 μg/mL carbenicillin and cultured at 37 °C overnight. The expression was stopped at an optical density at 600 nm of ~ 2.7.

Isolation of curli fibers using vacuum filtration. After the protein expression step, isolation of the curli-like proteins was conducted based on an established protocol.[6] Briefly, before the filtration,

the cultures were incubated with guanidinium chloride (GdmCl, final concentration of 0.8 M) for 20 min at 4 °C. 50 mL of the GdmCl-containing cultures were then vacuum-filtered onto 47 mm polycarbonate filter membranes with 10 µm pores (Thermo Fisher). The filtered biomass was subjected to three steps of incubation including; 1) 5 mL of 8 M GdmCl for 5 min, 2) 5 mL of an aqueous solution of Benzonase nuclease (Sigma-Aldrich, 1.5 U/ mL) for 10 min, and 3) 5 mL of 5% (m/v) sodium dodecyl sulfate (SDS) in water for 5 min. Each step was followed by 3 rinses with 5 mL of DI water. Semi-purified curli-like proteins were collected from the filter membrane by gently scraping the filter with a flat spatula. They were then lyophilized, and stored at 4 °C. However, filtration of the R1/R5 protein demanded a slight modification to the original protocol. To provide milder filtration conditions for R1/R5 proteins, which aggregated less than WT and R1/HAP/R5 proteins, the cultures were filtered without performing the 20-min pre-incubation step with GdmCl, and with a shorter incubation time (3 min) for all the reagents during the filtration process.

Assessment of Curli Expression. The first step to confirm the curli nanofiber expression was performed using the binding affinity of Congo Red dye to amyloid proteins.[6] 1-mL samples were taken directly from the bacteria cultures and centrifuged. The collected pellet was resuspended in phosphate buffer and incubated with Congo Red (final concentration of 0.00015% (m/v)) for 10 min. After a centrifugation step, absorbance of the supernatant was measured at 490 nm to quantify the amount of Congo Red that did not bind to the cells. After vacuum filtration, the deposition of curli nanofibers on the filter membranes was also assessed by incubating the filters in 5 mL of 0.015% (m/v) of Congo Red dye solution for 10 min, followed by vacuum filtration of the liquid and 3 rinses with 5 mL of DI water.

SDS-PAGE. The expression of the modified curli proteins was assessed by confirming their molecular weights using SDS-PAGE. 0.5 mg of curli proteins were disassembled by dissolving them in a 1:1 (v/v) Hexafluoroisopropanol:Trifluoroacetic acid (HFIP:TFA) (Oakwood Chemical) mixture and sonication for 1 h. After evaporating the solvent, the samples were resuspended in DI water and loading buffer. After electrophoresis at 200 V for 30 min, the gel was stained using Coomassie blue for 30 min, destained for 1 h, and imaged.

Electron Microscopy of bacterial cultures. Scanning electron microscopy (SEM) samples were prepared by depositing the samples, taken directly from bacterial culture, on 0.2 μm polycarbonate filter membranes (Whatman® Nuclepore from Millipore Sigma). The membranes were washed with 0.1 M sodium cacodylate buffer (Electron Microscopy Sciences), fixed with 2% (v/v) glutaraldehyde (Bio Basic) and 2% (v/v) paraformaldehyde (Electron Microscopy Sciences) for 2 h at room temperature, and solvent-exchanged sequentially in 0%, 25%, 50%, 75%, and 100% (v/v) ethanol (for 15 min in each solvent). The membranes were dried in a critical point dryer (CPD) and sputtered until they were coated with a 5 nm layer of Pt. Imaging was performed using a FEI Quanta 450 ESEM at 5 kV.

Fibrillation analysis of the modified CsgA monomers. Atomic force microscopy (AFM) was used to study the nanostructure of the disassembled curli-like nanofibers and their growth behavior during reassembly. The lyophilized proteins (0.5 mg/ml) were re-solubilized in 1 mL HFIP:TFA (1:1) and sonicated for 15 min. The stock solutions were diluted three times in DI water. After different incubation times, 4 μL of the protein solutions was added onto freshly cleaved mica sheets and allowed to dry overnight. The samples were imaged using a Veeco Multimode Nanoscope III AFM with a 240AC-NA micro cantilever tip (Opus).

Circular Dichroism (CD) spectroscopy. To evaluate the secondary structure of the engineered proteins, they were assayed in a Chirascan spectrophotometer (Applied Photophysics) from 180 to 260 nm in a quartz cell with a 1-mm path length at 20 °C, using 1 nm step size and a bandwidth of 1 nm. The protein solutions were prepared by immersing 0.5 mg of the proteins in 1 mL DI water overnight, followed by vigorous vortexing. Since curli fibers do not fully dissolve in water, the true concentrations of dissolved proteins in the CD cuvettes were calculated using the absorbance (A_{280}) of the solutions and their extinction coefficients predicted by Benchling (The Life Sciences R&D Cloud) at 280 nm. The molar ellipticity values were normalized by the concentration for each protein. All spectra were baseline corrected with respect to DI water.

Molecular dynamics modeling of the structure of truncated CsgA. To construct the mutant R1/R5 model, the sequence of the R1 and R5 repeats in CsgA was mapped onto R1 and R2 repeat structures from the predicted model introduced in reference 19.[37] The mapping was completed using MODELLER [38] and produced a monomer of 64 residues containing two β-strand repeats and a flexible 22-residue N-terminus. Next, the R1/R5 monomers were stacked into a multimer by aligning the interface between R1 of one monomer and R5 of another monomer to the same R1-R5 interface of the CsgA dimers created in reference 21.[39] This procedure was repeated to build multimer structures made up of 6 stacked monomers. A similar R1/HAP/R5 mutant model was also created by using MODELLER to insert the HAP sequence between R1 and R5 and multimers were built using the same steps as above.

Both multimer structures first underwent energy minimization for 12,000 steps using the conjugate gradient method and equilibration for 1.2 ns with all backbone atoms fixed excluding the 22-residue N-terminus and HAP insertion. Next, both structures underwent equilibration for

an additional 5 ns with no atoms fixed. Simulations were conducted using the Generalized Born Implicit Solvent as implemented in NAMD.[40] The alpha cutoff used was 15 Å and the ion concentration 0.05 molar, with solvent accessible surface area (SASA) calculations on. Simulations were run under the NVT ensemble with at 1 fs timestep and temperature of 300K. The latest CHARMM 36 parameter set is used.[41-43]

Mineralization of HAP crystals onto curli-like fibers and their characterization. To mineralize the proteins, 0.5 mg of the lyophilized proteins was dissolved in the mixture of the 100 µL of the 100 mM $CaCl_2$ and 100 µL of the 50 mM Na_2HPO_4 solution and incubated overnight at 37 °C. To remove excess salts, the samples were centrifuged and washed thorough 0.2 µm filter membranes. To investigate the morphology of the mineralized proteins using SEM, 50 µL of the mineralized protein solution was deposited on 0.2 µm polycarbonate filter membrane and rinsed with DI water. The samples were fixed using the protocol described above for bacterial cultures, dried by CPD, and sputtered coated by a 5 nm layer of Pt. In addition, mineralized samples were lyophilized and analyzed to confirm the formation of the HAP crystals using X-ray diffraction (XRD; Bruker D8 Discovery X-Ray Diffractometer (VANTEC Detector, Cu-Ka (alpha)).

Furthermore, the HAP nucleation ability of the modified proteins was studied by directly mineralizing the proteins on a TEM grid to minimize the effects of sample preparation, adapting an approach previously reported. 7 µL of protein solution (0.5 mg/L) was applied over a carbon coated TEM grid (200 mesh) for 2 min. The protein loaded TEM grid was then treated with 10 µL of 5 mM Na_2HPO_4 on one side and 10 µL of 10 mM $CaCl_2$ on the other side. After 2 h, the TEM grid was washed three times by dipping the grid in DI water and dried under ambient conditions before TEM analysis. A control sample without protein was also prepared and underwent the

same mineralization treatment. Transmission electron microscopy (TEM; FEI Tecnai G2 F20 200 kV Cryo-STEM) was used to observe the formation of the nucleated HAP minerals on the protein templates.

Conclusion

With their ability to self-assemble and to tolerate genetic modifications, CsgA proteins are promising candidates for fabrication of the protein-based materials for a wide variety of applications. Herein, we analyzed the functionality and self-assembly ability of the CsgA-like proteins after removing the internal repeats (R2-R4) and replacing them with a HAP-binding peptide. We obtained detailed information about the fibrillation and mineralization of the modified CsgA. We observed a fibrillar structure for R1/R5 and R1/HAP/R5 proteins, supporting the fact that R1 and R5 are the necessary aggregation prone repeats to form fibers. We confirmed the functionality of the incorporated HAP-binding peptide after mineralization of the modified proteins, and we assessed the formation of the HAP crystals. Overall, the resulting HAP-containing hydrogels are potential candidates for bone tissue engineering applications requiring porous and densely HAP-mineralized 3D scaffolds.

Further, we showed that reducing the CsgA proteins into R1/R5 complementary self-assembling monomers is a means to genetically assist in the self-assembly of a short functional peptide into a fibrous structure. This method circumvents the needs for post-processing chemical conjugation reactions that are traditionally required to attach free peptides to larger molecular scaffolds. Our new self-assembly tool thus brings an opportunity to repurpose free peptides as functional

supramolecules to produce functional fibrous materials and hydrogels for a wide range of the applications, ranging from biotechnology, to tissue engineering, and energy.

Aside from assisting the assembly of the free peptides and increasing the density of the active sites within a material, the fibers that we have engineered here also share many fascinating properties of the native curli system of *E. coli*. The truncated curli materials form hydrogels with a high genetic customizability, that can resist harsh processing conditions, and can be isolated from bacterial cultures in macroscopic quantities. The versatile processability of these materials makes them suitable for fabrication of the proteins-based materials in different forms, such as films, hydrogels, and aerogels. Besides, the curli system can be used as scaffold to introduce different functional peptides to tune its physicochemical properties for a wide variety of applications.

Author Information

Corresponding Author

Noémie-Manuelle Dorval Courchesne - Department of Chemical Engineering, McGill University, Montréal, QC, Canada

Email: Noemie.dorvalcourchesne@mcgill.ca

Authors

Zahra Abdali - Department of Chemical Engineering, McGill University, Montréal , QC, Canada

Masoud Aminzare - Department of Chemical Engineering, McGill University, Montréal , QC, Canada

Xiaodan Zhu - Department of Chemical Engineering, McGill University, Montréal , QC, Canada

Elizabeth DeBenedictis - Department of Mechanical Engineering, Northwestern University, Evanston, IL, United States of America

Oliver Xie - Department of Chemical Engineering, McGill University, Montréal , QC, Canada

Sinan Keten - Department of Mechanical Engineering, Northwestern University, Evanston, IL, United States of America

Supporting Information: Table S1. Primers and sequences used in this study, Figure S1. DNA and protein sequences for CsgA and modified CsgA constructs, Figure S2. Images for protein hydrogels, Figures S3 and S4. SEM images of mineralized protein hydrogels (protocol optimization and cross-sectional images).

Acknowledgments

This research was funded, in part, by the Natural Sciences and Engineering Research Council of Canada (NSERC) through a Discovery grant (NSERC RGPIN-2017-04598), and it was undertaken, thanks to the support by the Canadian Foundation for Innovation (project #37524). This work was also supported, in part, by an Établissement de nouveaux chercheurs universitaires FRQNT grant (FRQ-NT NC-255846). S.K. acknowledges funding from the Office of Naval Research Young Investigator Program (grant #N00014-15-1-2701). This work was also supported by two research

networks: the Québec Center for Advanced Materials (QCAM), and the Research Center for High Performance Polymer and Composite Systems (CREPEC), both supported by the FRQNT. Z.A. and M.A. are grateful for financial support by McGill Engineering Doctoral Awards (MEDA). O.X. is grateful for an NSERC Undergraduate Student Research Award. E.D.B. was additionally sponsored by the DoD, Air Force Office of Scientific Research, National Defense Science and Engineering Graduate (NDSEG) Fellowship, 32 CFR 168a. The authors acknowledge a supercomputing grant from the Northwestern University High Performance Computing Center and the Department of Defense Supercomputing Resource Center. E.D.B. gratefully acknowledges support from the Ryan Fellowship and the Northwestern University International Institute for Nanotechnology. The authors thank the Facility for Electron Microscopy and Research (FEMR) at McGill for assistance with SEM and TEM, and McGill Chemistry Microscopy and Imaging Lab (MIlab) for access to AFM facility.

References

[1] Barnhart, M. M., and Chapman, M. R. (2006) Curli biogenesis and function, *Annu Rev Microbiol. 60*, 131-147.

[2] Blanco, L. P., Evans, M. L., Smith, D. R., Badtke, M. P., and Chapman, M. R. (2012) Diversity, biogenesis and function of microbial amyloids, *Trends Microbiol. 20*, 66-73.

[3] Dorval Courchesne, N. M., DeBenedictis, E. P., Tresback, J., Kim, J. J., Duraj-Thatte, A., Zanuy, D., Keten, S., and Joshi, N. S. (2018) Biomimetic engineering of conductive curli protein films, *Nanotechnology. 29*, 454002-454013.

[4] Praveschotinunt, P., Dorval Courchesne, N. M., den Hartog, I., Lu, C., Kim, J. J., Nguyen, P. Q., and Joshi, N. S. (2018) Tracking of Engineered Bacteria In Vivo Using Nonstandard Amino Acid Incorporation, *ACS Synth Biol. 7*, 1640-1650.

[5] Duraj-Thatte, A. M., Dorval Courchesne, N. M., Praveschotinunt, P., Rutledge, J., Lee, Y., Karp, J. M., and Joshi, N. S. (2019) Genetically Programmable Self-Regenerating Bacterial Hydrogels, *Adv Mater. 31*, 1901826-1901835.

[6] Dorval Courchesne, N. M., Duraj-Thatte, A., Tay, P. K. R., Nguyen, P. Q., and Joshi, N. S. (2016) Scalable Production of Genetically Engineered Nanofibrous Macroscopic Materials via Filtration, *ACS Biomater. Sci. Eng. 3*, 733-741.
[7] Nguyen, P. Q. (2017) Synthetic biology engineering of biofilms as nanomaterials factories *Biochem. Soc. Trans. 45*, 585–597
[8] Nguyen, P. Q., Botyanszki, Z., Tay, P. K., and Joshi, N. S. (2014) Programmable biofilm-based materials from engineered curli nanofibres, *Nat Commun 5*, 4945-4955.
[9] Wang, X., Hammer, N. D., and Chapman, M. R. (2008) The molecular basis of functional bacterial amyloid polymerization and nucleation, *J Biol Chem. 283*, 21530-21539.
[10] Gilbert, C., and Ellis, T. (2019) Biological Engineered Living Materials: Growing Functional Materials with Genetically Programmable Properties, *ACS Synth Biol. 8*, 1-15.
[11] Schmieden, D. T., Basalo Vazquez, S. J., Sanguesa, H., van der Does, M., Idema, T., and Meyer, A. S. (2018) Printing of Patterned, Engineered E. coli Biofilms with a Low-Cost 3D Printer, *ACS Synth Biol. 7*, 1328-1337.
[12] Cui, M., Qi, Q., Gurry, T., Zhao, T., An, B., Pu, J., Gui, X., Cheng, A. A., Zhang, S., Xun, D., Becce, M., Briatico-Vangosa, F., Liu, C., Lu, T. K., and Zhong, C. (2019) Modular genetic design of multi-domain functional amyloids: insights into self-assembly and functional properties, *Chem Sci 10*, 4004-4014.
[13] Chung, W. J., Kwon, K. Y., Song, J., and Lee, S. W. (2011) Evolutionary screening of collagen-like peptides that nucleate hydroxyapatite crystals, *Langmuir. 27*, 7620-7628.
[14] Xu, B., Zheng, P., Gao, F., Wang, W., Zhang, H., Zhang, X., Feng, X., and Liu, W. (2017) A Mineralized High Strength and Tough Hydrogel for Skull Bone Regeneration, *Adv. Funct. Mater. 27*, 1604327.
[15] Fang, J., Li, P., Lu, X., Fang, L., Lu, X., and Ren, F. (2019) A strong, tough, and osteoconductive hydroxyapatite mineralized polyacrylamide/dextran hydrogel for bone tissue regeneration, *Acta Biomater. 88*, 503-513.
[16] Li, C., Born, A. K., Schweizer, T., Zenobi-Wong, M., Cerruti, M., and Mezzenga, R. (2014) Amyloid-hydroxyapatite bone biomimetic composites, *Adv Mater 26*, 3207-3212.
[17] Liu, C., Han, Z., and Czernuszka, J. T. (2009) Gradient collagen/nanohydroxyapatite composite scaffold: development and characterization, *Acta Biomater. 5*, 661-669.
[18] Shao, C., Zhao, R., Jiang, S., Yao, S., Wu, Z., Jin, B., Yang, Y., Pan, H., and Tang, R. (2018) Citrate Improves Collagen Mineralization via Interface Wetting: A Physicochemical Understanding of Biomineralization Control, *Adv Mater. 30*, 1704876.
[19] Raymond, D. M., and Nilsson, B. L. (2018) Multicomponent peptide assemblies, *Chem Soc Rev. 47*, 3659-3720.
[20] Jeffrey D. Hartgerink, E. B., Samue. (2001) Self-Assembly and Mineralization of Peptide-Amphiphile Nanofibers, *Science. 294*, 1684-1688.
[21] Chen, J., and Zou, X. (2019) Self-assemble peptide biomaterials and their biomedical applications, *Bioact Mater 4*, 120-131.
[22] Rivas, M., Del Valle, L. J., Aleman, C., and Puiggali, J. (2019) Peptide Self-Assembly into Hydrogels for Biomedical Applications Related to Hydroxyapatite, *Gels. 5*, 14-43.
[23] Jin, H. E., Jang, J., Chung, J., Lee, H. J., Wang, E., Lee, S. W., and Chung, W. J. (2015) Biomimetic Self-Templated Hierarchical Structures of Collagen-Like Peptide Amphiphiles, *Nano Lett. 15*, 7138-7145.
[24] Mahato, A., Sandy, Z., Bysakh, S., Hupa, L., Das, I., Bhattacharjee, P., Kundu, B., De, G., Nandi, S. K., Vallittu, P., Balla, V. K., and Bhattacharya, M. (2020) Development of nano-porous hydroxyapatite coated e-glass for potential bone-tissue engineering application: An in vitro approach, *Mater. Sci. Eng. C. 111*, 110764.

[25] Calabro, E. (2016) Competition between hydrogen bonding and protein aggregation in neuronal-like cells under exposure to 50 Hz magnetic field, *Int J Radiat Biol. 92*, 395-403.
[26] Dueholm, M. S., Nielsen, S. B., Hein, K. L., Nissen, P., Chapman, M., Christiansen, G., Nielsen, P. H., and Otzen, D. E. (2011) Fibrillation of the major curli subunit CsgA under a wide range of conditions implies a robust design of aggregation, *Biochemistry. 50*, 8281-8290.
[27] Tufail, S., Sherwani, M. A., Shoaib, S., Azmi, S., Owais, M., and Islam, N. (2018) Ovalbumin self-assembles into amyloid nanosheets that elicit immune responses and facilitate sustained drug release, *J Biol Chem 293*, 11310-11324.
[28] Hammer, N. D., McGuffie, B. A., Zhou, Y., Badtke, M. P., Reinke, A. A., Brannstrom, K., Gestwicki, J. E., Olofsson, A., Almqvist, F., and Chapman, M. R. (2012) The C-terminal repeating units of CsgB direct bacterial functional amyloid nucleation, *J Mol Biol. 422*, 376-389.
[29] Wang, X., Zhou, Y., Ren, J. J., Hammer, N. D., and Chapman, M. R. (2010) Gatekeeper residues in the major curlin subunit modulate bacterial amyloid fiber biogenesis, *Proc Natl Acad Sci U S A. 107*, 163-168.
[30] Qi, Q., Zhao, T. X., An, B. L., Liu, X.Y., Zhong, C. (2017) Self-assembly and morphological characterization of two-component functional amyloid proteins, *Chin. Chem. Lett. 28*, 1062-1068.
[31] Brown, P. D. (2017) Structural Characterization, In *Springer Handbook of Electronic and Photonic Materials.* (S. Kasap, P. C., Ed.), pp 385-412, Springer, Cham.
[32] Poralan, G. M., Gambe, J. E., Alcantara, E. M., and Vequizo, R. M. (2015) X-ray diffraction and infrared spectroscopy analyses on the crystallinity of engineered biological hydroxyapatite for medical application, *IOP Conf Ser Mater Sci Eng. 79*, 012028.
[33] Tavafoghi, M., and Cerruti, M. (2016) The role of amino acids in hydroxyapatite mineralization, *J R Soc Interface. 13*, 20160462.
[34] Kalaiselvi, V., Mathammal, R., Vijayakumar, S., and Vaseeharan, B. (2018) Microwave assisted green synthesis of Hydroxyapatite nanorods using Moringa oleifera flower extract and its antimicrobial applications, *Int J Vet Sci Med. 6*, 286-295.
[35] Song, F., Zhang, H., Wang, S., Liu, L., Tan, X., and Liu, S. (2018) Atomic-level design of CoOH(+)-hydroxyapatite@C catalysts for superfast degradation of organics via peroxymonosulfate activation, *Chem Commun (Camb). 54*, 4919-4922.
[36] Wei, G., Zhang, J., Xie, L., and Jandt, K. D. (2011) Biomimetic growth of hydroxyapatite on super water-soluble carbon nanotube-protein hybrid nanofibers, *Carbon. 49*, 2216-2226.
[37] DeBenedictis, E. P., Ma, D., and Keten, S. (2017) Structural predictions for curli amyloid fibril subunits CsgA and CsgB, *RSC Adv. 7*, 48102-48112.
[38] Eswar, N., Webb, B., Marti-Renom, M. A., Madhusudhan, M. S., Eramian, D., Shen, M. Y., Pieper, U., and Sali, A. (2006) Comparative protein structure modeling using Modeller, *Curr Protoc Bioinformatics. 47*, 5.6.1-32.
[39] Dunbar, M., DeBenedictis, E., and Keten, S. (2019) Dimerization energetics of curli fiber subunits CsgA and CsgB, *Npj Comput. Mater. 5*, 27-36.
[40] James C. Phillips, R. B., Wei Wang, James Gumbart, Emad Tajkhorshid, Elizabeth Villa, Christophe Chipot, Robert D. Skeel, Laxmikant Kalé, and Klaus Schulten. (2005) Scalable Molecular Dynamics with NAMD, *J Comput Chem. 26*, 1781–1802.
[41] A. D. MacKerell, J., D. Bashford, M. Bellott, R. L. Dunbrack, Jr., D. Evanseck, M. J. Field, S. Fischer, J. Gao, H. Guo, S. Ha, D. Joseph-McCarthy, L. Kuchnir, K. Kuczera, F. T. K. Lau, C. Mattos, S. Michnick, T. Ngo, D. T. Nguyen, B. Prodhom, W. E. Reiher, B. Roux, M. Schlenkrich, J. C. Smith, R. Stote, J. Straub, M. Watanabe, J. Wio´rkiewicz-Kuczera, D. Yin, and M. Karplus. (1998) All-Atom Empirical Potential for Molecular Modeling and Dynamics Studies of Proteins, *J. Phys. Chem. B. 102*, 3586-3616.

[42] Best, R. B., Zhu, X., Shim, J., Lopes, P. E., Mittal, J., Feig, M., and Mackerell, A. D., Jr. (2012) Optimization of the additive CHARMM all-atom protein force field targeting improved sampling of the backbone phi, psi and side-chain chi(1) and chi(2) dihedral angles, *J Chem Theory Comput. 8*, 3257-3273.

[43] Alexander D. MacKerell, J., Michael Feig, and Charles L. Brooks. (2004) Improved Treatment of the Protein Backbone in Empirical Force Fields, *J. Am. Chem. Soc. 126*, 698-699.